Electronic structure of a borophene layer in rare-earth aluminum/chromium boride and its hydrogenated derivative borophane

Masahito Niibe,[1,2] Mathis Cameau,[2,3,4] Nguyen Thanh Cuong,[5] Omeji Ilemona Sunday,[2,6] Xiaoni Zhang,[2] Yuki Tsujikawa,[2] Susumu Okada,[5] Kunio Yubuta,[7] Takahiro Kondo,[5] and Iwao Matsuda[2]

[1]*Laboratory of Advanced Science and Technology for Industry, University of Hyogo, 3-1-2 Koto, Kamigori-cho, Ako-gun, Hyogo 678-1205, Japan*

[2]*Institute for Solid State Physics (ISSP), The University of Tokyo, Kashiwa, Chiba 277-8581, Japan*

[3]*Institut des NanoSciences de Paris, Sorbonne Université, F-70005 Paris, France*

[4]*Institut de Minéralogie, de Physique des Matériaux et de Cosmochimie, Sorbonne Université, F-70005 Paris, France*

[5]*Faculty of Pure and Applied Sciences, University of Tsukuba, Tsukuba, Ibaraki 305-8571, Japan*

[6]*Université Jean Monnet, Saint-Étienne 42100, France*

[7]*Institute for Materials Research, Tohoku University, Sendai, Miyagi 980-8577, Japan*

(Received 27 August 2020; accepted 27 July 2021; published 23 August 2021)

We studied electronic states of borophene in a crystal of rare-earth aluminum/chromium boride and the hydrogenated sheet, borophane, successfully prepared by ion exchange and liquid exfoliation of the crystal. The layer has a boron network with five-membered and seven-membered rings. Electronic structures of all the boron-derived layers are found to be gapless by soft x-ray absorption and emission spectroscopy measurements at the B *K*-shell absorption edge and density functional theory calculations. The present results support the existence of a Dirac nodal loop at the Fermi level in the borophane layer with five- and seven-membered rings, predicted recently by topological calculations.

DOI: 10.1103/PhysRevMaterials.5.084007

I. INTRODUCTION

Varieties of two-dimensional materials have been predicted and synthesized, showing novel physical and chemical properties that have led to innovations in science and technology [1]. Well-known examples are layers of Xene that are composed of a single element, such as graphene (C) [2], silicene (Si) [3–7], germanene (Ge) [8–10], borophene (B) [11–15], and phosphorene (P) [16]. Recently, a freestanding sheet of hydrogen-terminated borophene, referred to as HB or borophane, was prepared by hydrogen adsorption of the surface borophene [17] or from a MgB_2 crystal using proton ion-exchange and liquid exfoliation procedures [18]. A boron sheet in MgB_2 forms a honeycomb lattice, and the resulting borophane is also composed of six-membered rings. The layers of borophane have shown useful functionalities such as metallic conduction [19,20], catalytic activity [21], metal ion reducibility [22], and a light response hydrogen release property [23]. On the other hand, it has been known that a series of the $RAlB_4$-type compounds, such as rare-earth aluminum/chromium borides, contain a peculiar boron network of five- and seven-membered rings [24]. Such layers of borophane are predicted to be semimetal with topological Dirac nodal loops (DNLs) [25]. Two-dimensional materials with DNL fermions are now the focus of this field to realize an exciting platform for exploring the exotic properties of Dirac fermions and designing novel quantum electronic devices at the nanoscale. Thus it is highly called for to examine electronic states in borophenes of five- and seven-membered rings in the $RAlB_4$-type crystals and also in borophane, isolated after the hydrogenation.

In the present research, we studied boron $2p$ states of the boron sheets in crystals of rare-earth aluminum/chromium borides and in borophane, exfoliated from the crystal with hydrogenation. We made measurements of soft x-ray absorption and emission (SXA and SXE) spectroscopies at the B *K* edge that has been useful to investigate boron-specific electronic states [26,27]. The experimental results of the $R(Al_{0.95}Cr_{0.05})B_4$ crystals (R = Tm, Yb, Lu) showed that the electronic states are gapless. The electronic calculation revealed that there is charge transfer from metal atoms to the boron layers and there is also notable variation of the B p_z state. We have also succeeded in preparing hydrogenated boron sheets, i.e., HB or borophane, from crystals of rare-earth aluminum/chromium boride by the proton ion-exchange and exfoliation methods. Electronic states of a HB sheet or borophane were found to be gapless and reproduced by density functional theory (DFT) calculations. The consistency between experiments and calculations indicates that borophane with five- and seven-membered rings is (semi)metallic, and it supports the existence of the Dirac nodal fermions in the material.

II. EXPERIMENTAL AND CALCULATION METHODS

Three rare-earth (aluminum/chromium) boride crystals, $Tm(Al_{0.95}Cr_{0.05})B_4$, $Yb(Al_{0.95}Cr_{0.05})B_4$, and $Lu(Al_{0.95}Cr_{0.05})B_4$, were synthesized based on the self-flux growth method as follows [24]. A more detailed description is given in Appendix A. A photograph of synthesized $Yb(Al_{0.95}Cr_{0.05})B_4$ single crystals is shown in Fig. 1(a). The crystal size is as small as 1 mm and has a metallic

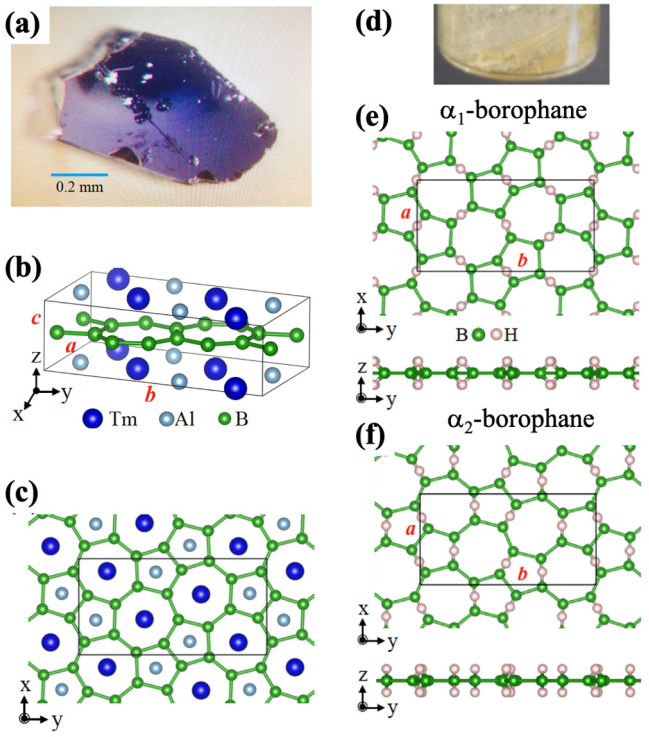

FIG. 1. (a) A photograph of a single crystal of $Yb(Al_{0.95}Cr_{0.05})B_4$. (b) and (c) Schematic drawings of the crystalline structure of $RAlB_4$ (R = Tm, Yb, Lu) in (b) oblique perspective view and (c) projected along the [001] direction. Ultramarine, light blue, and green balls represent Tm, Al, and B atoms, respectively. (d) A photograph of HB powders of the (5-7)-borophane layers. (e) and (f) Atomic structures of (5-7)-α_1-borophane monolayer (e) and (5-7)-α_2-borophane monolayer (f). Boron and hydrogen atoms are shown as green and white balls, respectively, while the unit cell is shown by the solid line.

luster. Such $RAlB_4$-type crystals have a layered structure consisting of metal layers and atomic sheets of boron, as shown in Figs. 1(b) and 1(c). The network structure of boron is a unique one, forming alternative arrangements of five- and seven-membered rings (the space group is *Pbam*) [24], making it the perfect mother material for the five- and seven-membered ring borophane.

Hydrogenation of boron sheets in crystals of rare-earth aluminum/chromium boride was conducted by the proton ion-exchange reaction, associated with liquid exfoliation. By reacting to protons in the solution, $YCrB_4$ or $TmAlB_4$ crystals were divided into sheets of HB and metal ions. After the reaction, HB sheets were contained in the supernatant liquid and, eventually, collected after drying [Fig. 1(d)]. The HB layer, borophane, consists of the five- and seven-membered ring boron sheets, (5-7)-borophene, in the $RAlB_4$-type crystal with hydrogen termination. Depending on the hydrogen configurations, two models, (5-7)-α_1-borophane and (5-7)-α_2-borophane, were proposed, as illustrated in Figs. 1(e) and 1(f), respectively. The ion-exchange method has been developed to synthesize honeycomb HB sheets from MgB_2 crystals [18]. A more detailed description of the present case is given in Appendix B.

Spectral measurements of B *K*-edge SXA and SXE were carried out using the undulator beamline BL-09A [28] at the NewSUBARU Synchrotron Radiation Facility at the University of Hyogo. The incident x-rays are linearly polarized in the horizontal plane at >99.6% [29]. The experiment was performed at room temperature. The total fluorescence yield (TFY) or the total electron yield (TEY) method can be used for the SXA measurement [30]. For SXE spectroscopy [31], the excitation photon energy was 210 eV, and the spectra were acquired at takeoff angles of 15°, 35°, and 60° from the sample surface. The crystalline sample was fixed so that the flat surface of the crystal was parallel to the surface of a sample holder. The total energy resolution of the SXE spectrometer in this region was 0.2 eV.

The geometric and electronic properties of materials were determined by first-principles calculations under the framework of DFT [32,33] using the Vienna *ab initio* simulation package (VASP) [34] with projected-augmented wave pseudopotentials [35]. The valence wave functions were expanded in terms of the plane-wave basis set with an energy cutoff of 520 eV. The generalized-gradient approximation proposed by the Perdew, Burke, and Ernzerhof functional [36] was used to express the exchange-correlation energy of interacting electrons. In the case of the $TmAlB_4$ crystal, the electronic properties of which were calculated in this paper, we used the DFT + Hubbard U method [37] with $U = 3$ eV to accurately describe the strong correlation behavior of the f electron of the rare-earth Tm element. All the internal atomic coordinates of the $TmAlB_4$ crystal were fully optimized at experimental lattice constants. A unit cell, shown in Fig. 1, had a size of $a = 5.9225$ Å, $b = 11.4784$ Å, and $c = 3.5224$ Å. For the isolated boron layers or the hydrogenated boron (borophane) sheets, a vacuum region of 15 Å was used to separate the periodic images. Both the internal atomic coordinates and lattice parameters of borophane were fully optimized. The Brillouin-zone integration was carried out using the Monkhorst-Pack k mesh [38] with a 0.01 $Å^{-1}$ spacing grid in the self-consistent field calculations for optimization structures. The orbital projected density of states was computed with a dense k mesh of 0.0035 $Å^{-1}$ spacing grid.

III. RESULTS AND DISCUSSION

A. Boron layers in the $RAlB_4$ crystal

Figure 2(a) shows SXA spectra at the B *K*-shell absorption edge of three types of $R(Al_{0.95}Cr_{0.05})B_4$ (R = Tm, Yb, Lu) crystals. An incident angle of the soft x-ray beam to the sample was set at 0°, measured from the surface normal. The SXA spectra of the three types of crystals are similar to each other. The energy at the absorption edge is as low as 187 eV, close to that of metallic boron [39,40]. Broad main peaks are found at 188.5 and 197.5 eV. Among the plural peaks, a peak at 194 eV is due to the oxidized impurity [41,42].

SXE spectra at the B *K* edge of three types of $R(Al_{0.95}Cr_{0.05})B_4$ crystals are collected in Fig. 2(b). There was no significant difference between the three sample crystals. A spectral edge of the emission spectrum on the higher-energy side was about 187 eV, which was close to that of the MgB_2 crystal or the HB monolayer sheet, reported in Refs. [18,19]. The broad main peak is at 183.5 eV with

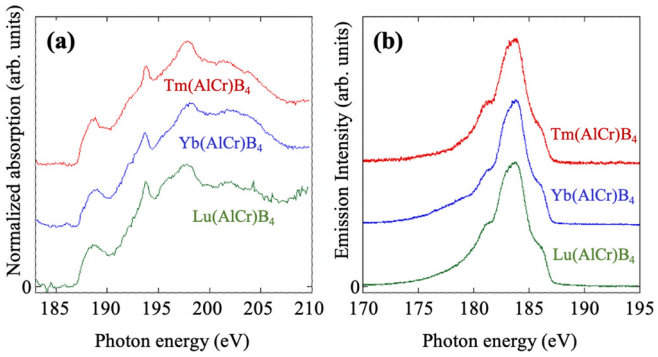

FIG. 2. (a) SXA and (b) SXE spectra of the three $R(Al_{0.95}Cr_{0.05})B_4$ crystals. The relation between the line color and the rare-earth metal species is denoted in the figure.

shoulders at 182 and 186 eV on both sides. In both SXA and SXE spectra, one finds similar spectral shapes for the three kinds of rare-earth metal borides.

To investigate the origins of electronic states in the spectra, Fig. 3(a) shows the total density of states (DOS) and the partial density of states (PDOS) of the B 2*s* and B 2*p* states of the $TmAlB_4$ crystal based on theoretical calculation.

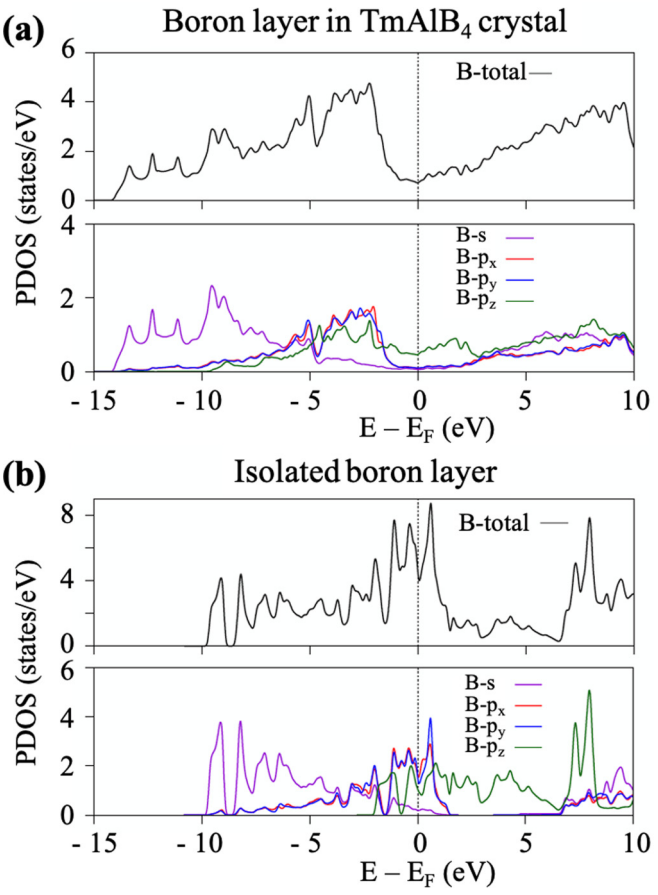

FIG. 3. Calculated electronic states of (a) the boron layer in the $TmAlB_4$ crystal and (b) the isolated boron layer having a network of five- and seven-membered rings. The spectra are the total density of states and the partial density of states of the B 2*s* and B 2*p* states.

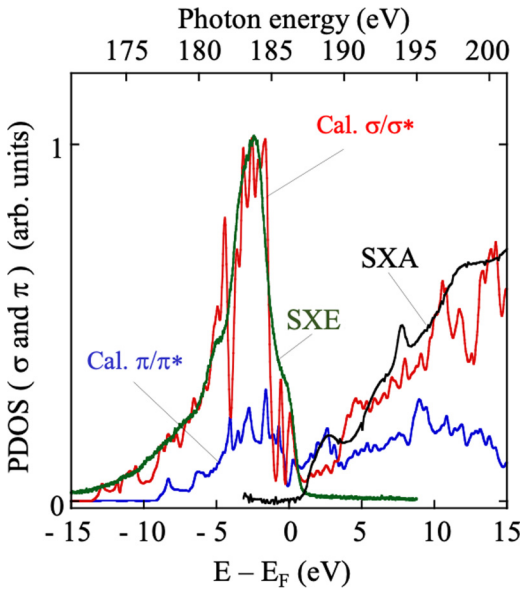

FIG. 4. The calculated (Cal.) ground state σ (σ^*) band and the π (π^*) band for the boron layer in the $TmAlB_4$ crystal are estimated from the atomic $(2p_x + 2p_y)$ and $2p_z$ orbitals' projected density of states of the boron layer. The SXA and SXE spectra of the $Yb(Al_{0.95}Cr_{0.05})B_4$ sample, taken around the magic angles, are superimposed in the figure.

For a comparison, results of the boron layer, isolated from the $TmAlB_4$ model, are shown in Fig. 3(b). Valence states of borophene with the five- and seven-membered rings are essentially composed of B 2*p* orbitals that make σ (p_x, p_y) and π (p_z) bonds. The DOSs of the boron layer are distributed to a higher binding energy in $TmAlB_4$ than that in the isolated one. This calculation result indicates that, in $TmAlB_4$, there exists charge transfer to the boron layers from metal atoms, as expected from their positive ionicity. In addition, the PDOS of the p_z orbital changed apparently due to the metal-boron interactions along the z direction, as found in the crystal structure in Figs. 1(b) and 1(c).

Figure 4 shows the calculated PDOS of the σ (σ^*) and π (π^*) bands of the boron layer in $TmAlB_4$. In the figure, the experimental data of the $Yb(Al_{0.95}Cr_{0.05})B_4$ sample are superimposed for comparison. As shown in Fig. 2, spectra of the $RAlB_4$-type crystals are similar to each other, and the $Yb(Al_{0.95}Cr_{0.05})B_4$ spectrum was chosen due to the best signal-to-noise ratio. Since the SXA and SXE spectra reflect the dipole transition between B 2*p* and B 1*s* states, the features correspond to the occupied 2*p* valence band (σ, π) and the unoccupied 2*p* conduction band (σ^*, π^*), respectively [26,43–45]. One can find in the figure that the calculated energy spectra agree well with the experimental data, including the spectral shoulders. It can be thus concluded that the electronic structure of the boron layer in the $TmAlB_4$-type crystal is gapless.

To further investigate spectral features of $RAlB_4$, the $Yb(Al_{0.95}Cr_{0.05})B_4$ spectra were measured at the various soft x-ray (SX) incident and takeoff angles, as shown in Fig. 5. Since the π and σ orbitals of the boron sheets are inherently orthogonal to each other, analysis of the dipole transition with

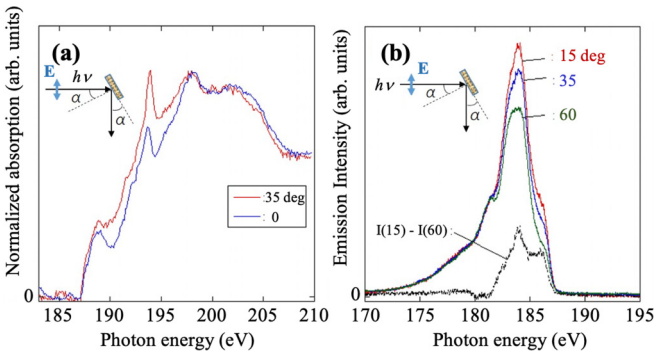

FIG. 5. Incident and takeoff angle dependence of (a) SXA and (b) SXE spectra of the $Yb(Al_{0.95}Cr_{0.05})B_4$ crystal. The intensities were normalized at 197.5 eV in SXA spectra [Fig. 5(a)] and at 182 eV in SXE spectra [Fig. 5(b)] to enhance features around the Fermi level. The incident angle was referred to the sample surface normal, while the takeoff angle was referred from the sample surface. The definition provides the same angle value, α, regardless of the sample rotation in the vertical axis. The intensity difference between SXE spectra at $\alpha = 15^\circ$ and 60°, I(15) − I(60), is drawn with a dashed black line.

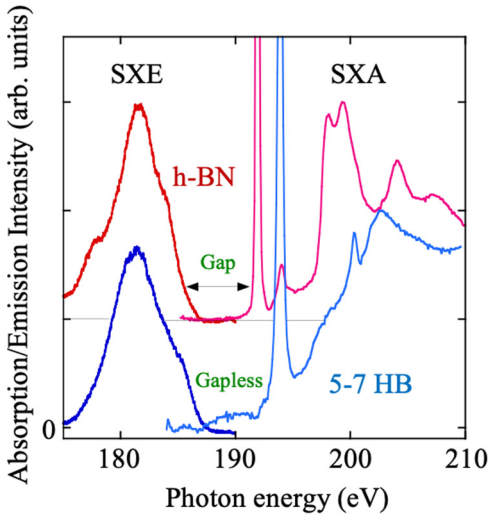

FIG. 6. SXE and SXA spectra at the B *K*-edge region for borophane (HB) with the five- and seven-membered rings. As a reference, SXE and SXA spectra of the h-BN powder are also shown with a baseline.

linearly polarized light provides information on the orbital orientation and also its possible modification in a crystal. As presented in Fig. 5, both the SXA and SXE spectra have only slight changes with angle. This is in sharp contrast to the cases of layers of hexagonal boron nitride (h-BN) and highly oriented pyrolytic graphite (HOPG) [46–53], showing a large incident and takeoff angle dependence. The spectral behavior of the $Yb(Al_{0.95}Cr_{0.05})B_4$ crystal can be understood in two ways. (i) Both π and σ bands overlap each other in the SXA and SXE spectra, so that a net variation of the opposite angle dependence had little result. (ii) The B $2p_z$ orbital of the π band may be perturbed notably by interactions with the neighboring metal atoms in the crystal. Such spectral suppression of the intrinsic p_z orbital was previously reported in N *K*-edge SXE measurements in the h-BN/Ni(111) system [54,55].

In Fig. 5(b), the normalized SXE intensity around 185 eV decreases with takeoff angle. The behavior corresponds to the B π component. To enhance the spectral feature, a differential SXE spectrum was obtained by subtracting the intensity at the takeoff angle of $\alpha = 60^\circ$ from that at the takeoff angle of 15°, I(15) − I(60), as previously done for the h-BN system [49]. When the spectra are compared with those of the π component in the band calculation, shown in Fig. 4, it can be seen that the shapes substantially match with each other. This result indicates that not only the main peak but also the spectral edge, appearing as a peak shoulder at 186 eV, has a contribution of the B π state in $RAlB_4$. This is different from the SXE spectra of MgB_2,which have only the σ component at the SXE edge [26].

B. Layer of HB or borophane

Figure 6 shows the SXE and SXA spectra of the borophane layer taken at the B *K*-shell absorption edge. The SXA spectrum was recorded by the TEY method. It is of note that the surface-sensitive TEY method was adopted for measurements on a sample of the HB layer. For a comparison, spectra of the h-BN powder are also shown in the figure. The sharp peak at 192 eV is assigned to the π^* band of h-BN [39,42,53]. The SXE and SXA spectra show the photon energy region (∼187–192 eV) with no signal, corresponding to the energy gap. The h-BN layer is insulating and displays a band gap. On the other hand, the spectral intensity is apparently found at the corresponding range in the HB layer. An overlap of the SXE and SXA spectra indicates that the electronic state is gapless. An oxide peak of boron is observed at 194 eV due to surface oxidation by the inevitable exposure during the sample transport in air. Since the boron oxides are insulating, there is no electronic contribution in the gapless state.

In order to understand the electronic states, calculations were made on borophane layers of five- and seven-membered rings, as shown in Fig. 7. In the previous report, two types of the layers, α_1-borophane [Figs. 1(e) and 7(a)] and α_2-borophane [Figs. 1(f) and 7(b)], were theoretically found to be stable [25]. These atomic structures share the same borophene framework of the five- and seven-membered rings with different configurations of hydrogen atoms. The two borophane layers exhibit semimetallic behavior with the topological Dirac nodal loops that can be described in terms of the nonsymmorphic group and the Z_2 topology [25]. As shown in Fig. 7, in each case, calculation of the density of states confirms that there is no energy gap in the electronic structure. The PDOS calculation reveals that electronic states originate from B p states and the gapless feature is due to overlap of PDOS edges of the B p_z and B p_x, p_y orbitals, which is the nature of topological Dirac nodal loops. The DOS calculation reproduces overlaps of the SXE and SXA spectra in Fig. 8. The consistency between theory and experiment indicates semimetallicity of borophane with the five- and seven-membered rings and indirectly supports the existence of the Dirac nodal fermion in the material. Quantum states of novel Dirac nodal loops have recently attracted attention for intriguing physical properties, such as ultrahigh carrier

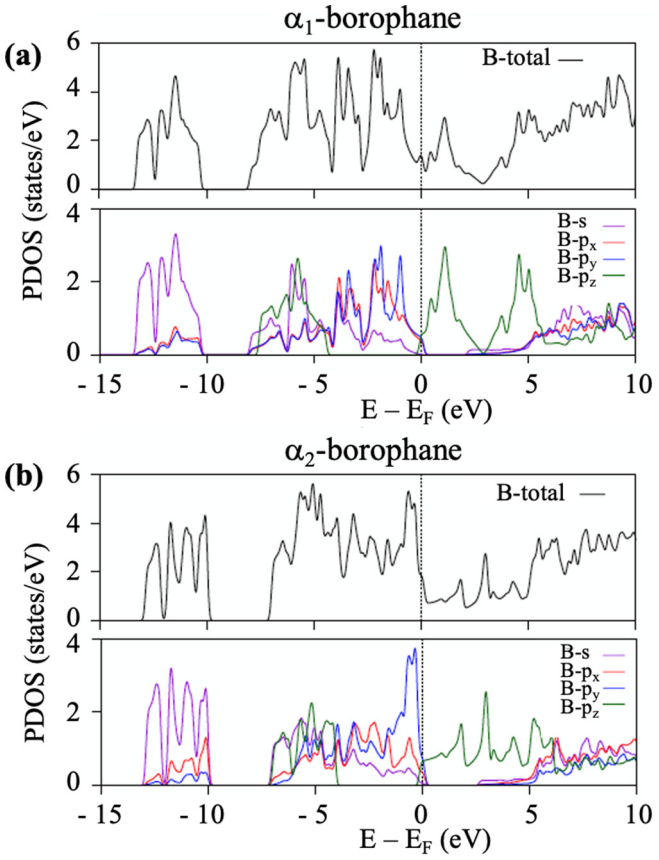

FIG. 7. Calculated total density of states and partial density of states of the (5-7)-α_1-borophane monolayer (a) and the (5-7)-α_2-borophane monolayer (b). The structure models are illustrated in Fig. 1. A unit cell of (5-7)-α_1-borophane [Fig. 1(e)] had size $a = 5.8752$ Å and $b = 11.2921$ Å, while that of (5 -7)-α_2-borophane [Fig. 1(f)] had size $a = 5.8293$ Å and $b = 11.3008$ Å in the calculation.

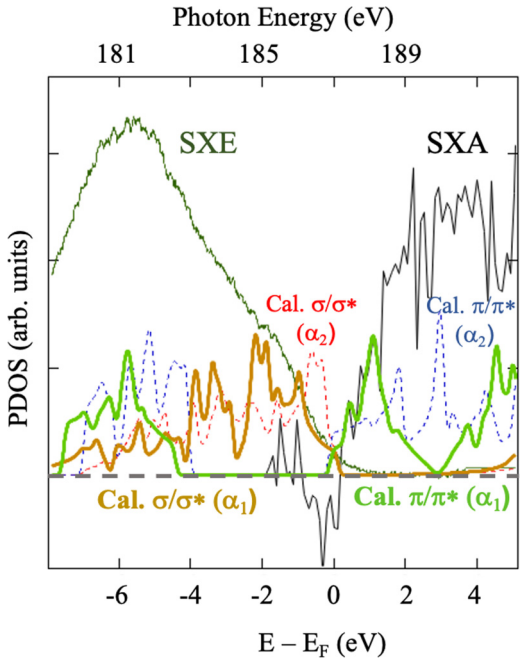

FIG. 8. The calculated σ/σ^* band and the π/π^* band for the borophane layer of the α_1 and α_2 types. The SXA and SXE spectra of the borophane sample are superimposed in the figure.

mobility or unique spin transport properties, expected from research [56,57]. Layers of borophane, studied in this paper, have a high potential to become a new and exciting platform for exploring the exotic behaviors of Dirac fermions and developing quantum devices [58].

Systematic comparisons of PDOSs between a boron layer in a crystal of rare-earth aluminum/chromium boride ($RAlB_4$), borophene (B), and borophane (HB) in Figs. 4 and 8 allow us to trace the electronic evolutions of the B p states through the ion-exchange reaction in Fig. 9. The valence electrons of boron atoms are distributed in p_x, p_y, and p_z states in these materials. In a borophene layer, σ (p_x, p_y) bands are mainly occupied, while π (p_z) bands are partly occupied. These PDOS spectra energetically overlap each other at the Fermi level, making the electronic structure gapless. When the boron sheet is sandwiched with metal atoms, as in the case of the $RAlB_4$ crystal, the σ band is almost completely occupied, leaving only the metallic π band. On the other hand, the hydrogenated borophene, HB, keeps both the σ and π bands at the Fermi level, making the system a topological nodal semimetal. All the boron layers of the five- and seven-membered rings individually have gapless states. On the other hand, it is intriguing to find their distinctive electronic characters with chemical environments. The present results of the experiments and calculations provide electronic information that can be used in designing functional materials related to borophene.

IV. SUMMARY

We investigated electronic structures of various boron layers with five- and seven-membered rings by soft x-ray absorption and emission (SXA and SXE) spectroscopies at the B K edges with DFT calculations. First, the borophene layers were studied for three crystals of the rare-earth aluminum/chromium borides $Tm(Al_{0.95}Cr_{0.05})B_4$, $Yb(Al_{0.95}Cr_{0.05})B_4$, and $Lu(Al_{0.95}Cr_{0.05})B_4$. Electronic structures of all the boron layers are found to be gapless, and the spectral features were similar to each other, indicating universal behavior of the B p states in the crystals. The theoretical calculation reproduced the experimental results and revealed that there exists charge transfer from metal atoms to the boron layers as well as a notable variation of the B p_z state. Rare-earth metal borides have shown varieties of quantum phenomena, such as magnetisms [24]. These results infer that the role of the boron layer is rather universal.

The present research has also succeeded in preparing hydrogenated boron sheets from crystals of rare-earth aluminum/chromium boride using proton ion-exchange and exfoliation methods. The B K-edge SXA and SXE measurements have found that the electronic states of sheets of HB, or borophane, are gapless. The DOS calculation of the sheet also shows gapless electronic states. The consistency between experimental SX spectra and theoretical PDOS calculation indicates semimetallicity of borophane with five- and seven-membered rings and indirectly supports the existence of the Dirac nodal fermion in the material.

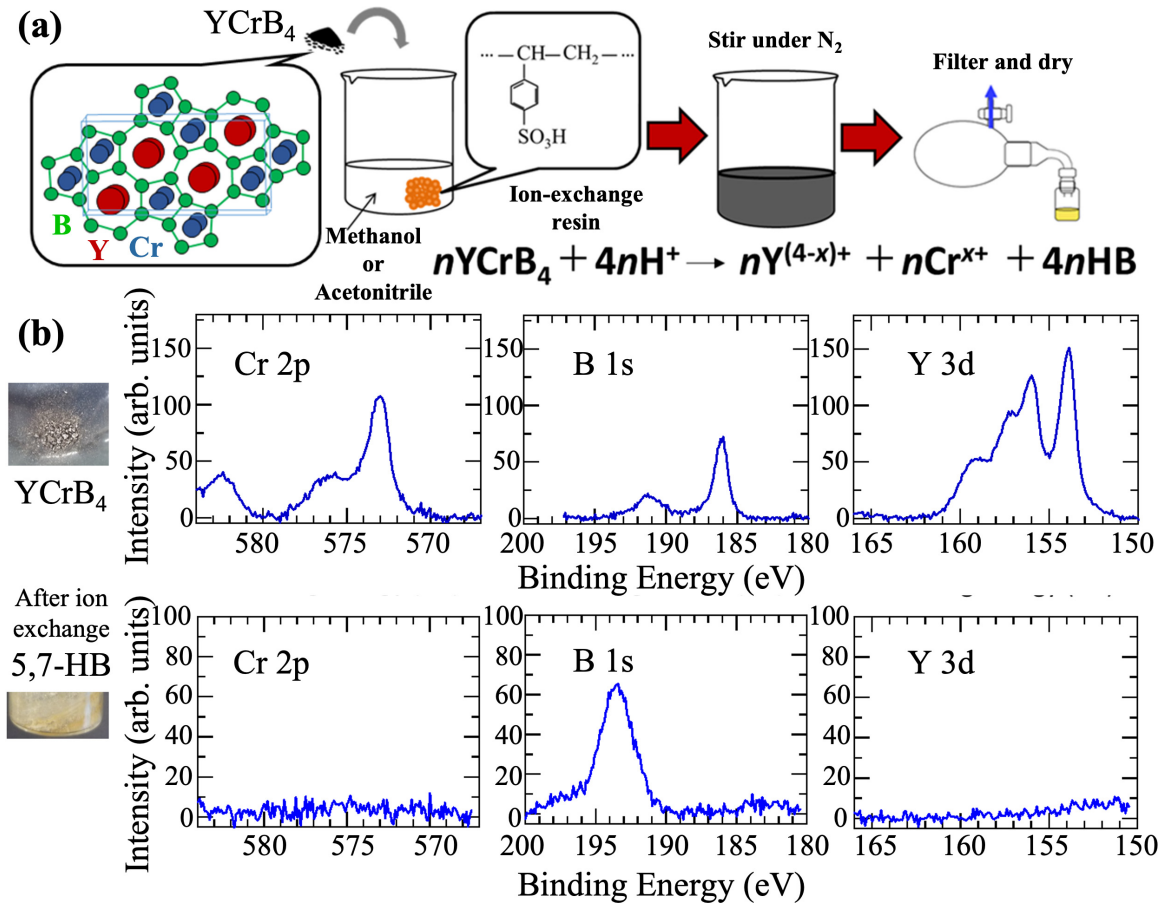

FIG. 9. (a) Schematic drawing of the preparation procedure of the borophane (HB) sheet: proton ion exchange and exfoliation. (b) Photographs and XPS spectra (Cr 2*p*, B 1*s*, and Y 3*d*) of the $YCrB_4$ crystal as the parent material and the borophane sheets, produced by the process.

ACKNOWLEDGMENTS

This work was partially supported by the NewSUBARU SR facility at the University of Hyogo and a Grant-in-Aid for Specially Promoted Research (KAKENHI Grants No. 18H03874, No. 19H04398, No. 18H03874, No. 19H02551, No. 19H05046:A01, and No. 21H05012). K.Y. was partly supported by JSPS KAKENHI Grants No. JP19K05643 and No. JP20H05258. T.K. appreciates the financial support from the MEXT Element Strategy Initiative to Form Core Research Centre (Grant No. JPMXP0112101001) and MHI Innovation Accelerator LLC. The preliminary experiments were carried out at SPring-8 BL07LSU of the Synchrotron Radiation Research Organization and the Institute for Solid State Physics, The University of Tokyo. In carrying out this research, Prof. Shigeru Okada at Kokushikan University and Ryota Ishibiki at University of Tsukuba sprovided support with the sample preparation, and Dr. Susumu Yamamoto at Tohoku University cooperated in cleaning the sample surfaces. M.N. was supported by the budget of a visiting professorship at the Institute for Solid State Physics, The University of Tokyo.

APPENDIX A: PREPARATIONS OF THE $RAlB_4$ CRYSTALS

For the preparation of the $RAlB_4$ crystals, the starting materials of the solids had a purity of 99.5–99.9% for R_2O_3 (R = Tm, Yb, Lu), Cr, and B, while the purity was 99.99% for Al. For the flux, atomic ratios of $B/R_2O_3 = 9.0$ ($R_2O_3 + 9B \rightarrow 2RB_3 + 3BO$) and mixed flux $Al_{1-x}Cl_x$ ($x = 0.050$) were used. Mixtures of the materials in the proper atomic ratios were placed in an Al_2O_3 crucible, heated in an Ar atmosphere at a soaking temperature of 1773 K for 5 h, and slowly cooled to room temperature at a rate of 50 K/h. Then, the sample crystals were separated from the solidified melts by dissolving the excess Al with diluted hydrochloric acid. At this stage, the compound, added with 5% Cr instead of pure Al, was used for stabilizing the phase.

APPENDIX B: PREPARATIONS OF THE HB SHEETS

The HB sheets were prepared by the ion-exchange method from crystals of the $RAlB_4$ type, such as $YCrB_4$ and $TmAlB_4$. In the case of the $YCrB_4$ crystal, the reaction can be described as $nYCrB_4 + 4nH^+ \rightarrow nY^{(4-x)+} + nCr^{x+} + 4nHB$, where HB represents hydrogen boride or borophane sheets with a stoichiometric ratio of B : H = 1 : 1 and n and x are integers with the relationship $4 > x \geqq 1$. Figure 9(a) schematically shows the synthesis, which consists of adding $YCrB_4$ powder to a methanol or acetonitrile solution with an ion-exchange resin and exfoliating in the solution. The process was done at room temperature under a nitrogen atmosphere. The supernatant liquid contained the HB sheets,

which were collected after drying. The HB layers consisted of the peeled boron layers with five- and seven-membered rings in an $YCrB_4$ crystal with hydrogen termination (borophane). The XPS spectra of the $YCrB_4$ powder, which is a synthetic raw material, and a HB sheet with five- and seven-membered rings are shown in Fig. 9(b). In the synthesized the HB sheet, core-level peaks of Cr 2*p* and Y 3*d* disappeared completely, meaning that the sample contained no metal element. The same preparation procedure was also available for HB sheets from the $TmAlB_4$ crystals.

[1] *Monatomic Two-Dimensional Layers: Modern Experimental Approaches for Structure, Properties, and Industrial Use*, edited by I. Matsuda (Elsevier, Amsterdam, 2019).

[2] A. H. Castro Neto, F. Guinea, N. M. R. Peres, K. S. Novoselov, and A. K. Geim, Rev. Mod. Phys. **81**, 109 (2009).

[3] P. Vogt, P. DePadova, C. Quaresima, J. Avila, E. Frantzeskakis, M. C. Asensio, A. Resta, B. Ealet, and G. Le Lay, Phys. Rev. Lett. **108**, 155501 (2012).

[4] A. Fleurence, R. Friedlein, T. Ozaki, H. Kawai, Y. Wang, and Y. Yamada-Takamura, Phys. Rev. Lett. **108**, 245501 (2012).

[5] C.-L. Lin, R. Arafune, K. Kawahara, N. Tsukahara, E. Minamitani, Y. Kim, N. Takagi, and M. Kawai, Appl. Phys. Express **5**, 045802 (2012).

[6] Y. Fukaya, I. Mochizuki, M. Maekawa, K. Wada, T. Hyodo, I. Matsuda, and A. Kawasuso, Phys. Rev. B **88**, 205413 (2013).

[7] B. Feng, H. Zhou, Y. Feng, H. Liu, S. He, I. Matsuda, L. Chen, E. F. Schwier, K. Shimada, S. Meng, and K. Wu, Phys. Rev. Lett. **122**, 196801 (2019).

[8] M. E. Davila, L. Xian, S. Cahangirov, A. Rubio, and G. LeLay, New J. Phys. **16**, 095002 (2014).

[9] C. H. Lin, A. Huang, W. W. Pai, W. C. Chen, T. Y. Chen, T. R. Chang, R. Yukawa, C. M. Cheng, C. Y. Mou, I. Matsuda, T. C. Chiang, H. T. Jeng, and S. J. Tang, Phys. Rev. Mater. **2**, 024003 (2018).

[10] Y. Fukaya, I. Matsuda, B. Feng I. Mochizuki, T. Hyodo, and S. Shamoto, 2D Mater. **3**, 035019 (2016).

[11] A. J. Mannix, X.-F. Zhou, B. Kiraly, J. D. Wood, D. Alducin, B. D. Myers, X. Liu, B. L. Fisher, U. Santiago, J. R. Guest, M. J. Yacaman, A. Ponce, A. R. Oganov, M. C. Hersam, and N. P. Guisinger, Science **350**, 1513 (2015).

[12] B. Feng, J. Zhang, R.-Y. Liu, T. Iimori, C. Lian, H. Li, L. Chen, K. Wu, S. Meng, F. Komori, and I. Matsuda, Phys. Rev. B **94**, 041408(R) (2016).

[13] B. Feng, O. Sugino, R.-Y. Liu, J. Zhang, R. Yukawa, M. Kawamura, T. Iimori, H. Kim, Y. Hasegawa, H. Li, L. Chen, K. Wu, H. Kumigashira, F. Komori, T.-C. Chiang, S. Meng, and I. Matsuda, Phys. Rev. Lett. **118**, 096401 (2017).

[14] B. Feng, J. Zhang, S. Ito, M. Arita, C. Cheng, L. Chen, K. Wu, F. Komori, O. Sugino, K. Miyamoto, T. Okuda, and S. Meng, Adv. Mater. (Weinheim) **30**, 1704025 (2018).

[15] S. Gupta, A. Kutrana, and B. I. Yakobson, Phys. Chem. Lett. **9**, 2757 (2018).

[16] H. Liu, A. T. Neal, Z. Zhu, Z. Luo, X. Xu, D. Tomanek, and P. D. Ye, ACS Nano **8**, 4033 (2014).

[17] Q. Li, V. S. C. Kolluru, M. S. Rahn, E. Schwenker, S. Li, R. G. Hennig, P. Darancet, M. K. Y. Chan, and M. C. Hersam, Science **371**, 1143 (2021).

[18] H. Nishino, T. Fujita, N. T. Cuong, S. Tominaka, M. Miyauchi, S. Iimura, A. Hirata, N. Umezawa, S. Okada, E. Nishibori, A. Fujino, T. Fujimori, S. Ito, J. Nakamura, H. Hosono, and T. Kondo, J. Am. Chem. Soc. **139**, 13761 (2017).

[19] I. Tateishi, N. T. Cuong, C. A. S. Moura, M. Cameau, R. Ishibiki, A. Fujino, S. Okada, A. Yamamoto, M. Araki, S. Ito, S. Yamamoto, M. Niibe, T. Tokushima, D. E. Weibel, T. Kondo, M. Ogata, and I. Matsuda, Phys. Rev. Mater. **3**, 024004 (2019).

[20] S. Tominaka, R. Ishibiki, A. Fujino, K. Kawakami, K. Ohara, T. Masuda, I. Matsuda, H. Hosono, and T. Kondo, Chem **6**, 406 (2020).

[21] A. Fujino, S. Ito, T. Goto, R. Ishibiki, J. Kondo, T. Fujitani, J. Nakamura, H. Hosono, and T. Kondo, ACS Omega **4**, 14100 (2019).

[22] S. Ito, T. Hirabayashi, R. Ishibiki, R. Kawamura, T. Goto, T. Fujita, A. Yamaguchi, H. Hosono, M. Miyauchi, and T. Kondo, Chem. Lett. **49**, 789 (2020).

[23] R. Kawamura, N. T. Cuong, T. Fujita, R. Ishibiki, T. Hirabayashi, A. Yamaguchi, I. Matsuda, S. Okada, T. Kondo, and M. Miyauchi, Nat. Commun. **10**, 4880 (2019).

[24] T. Mori, H. Borrmann, S. Okada, K. Kudou, A. Leithe-Jasper, U. Burkhardt, and Y. Grin, Phys. Rev. B **76**, 064404 (2007).

[25] N. T. Cuong, I. Tateishi, M. Cameau, M. Niibe, N. Umezawa, B. Slater, K. Yubuta, T. Kondo, M. Ogata, S. Okada, and I. Matsuda, Phys. Rev. B **101**, 195412 (2020).

[26] J. Nakamura, N. Yamada, K. Kuroki, T. A. Callcott, D. L. Ederer, J. D. Denlinger, and R. C. C. Perera, Phys. Rev. B **64**, 174504 (2001).

[27] Y. Zhu, A. R. Moodenbaugh, G. Schneider, J. W. Davenport, T. Vogt, Q. Li, G. Gu, D. A. Fischer, and J. Tafto, Phys. Rev. Lett. **88**, 247002 (2002).

[28] M. Niibe, M. Mukai, S. Miyamoto, Y. Shoji, S. Hashimoto, A. Ando, T. Tanaka, M. Miyai, and H. Kitamura, in *Synchrotron Instrumentation: Eighth International Conference on Synchrotron Radiation Instrumentation*, AIP Conference Proceedings Vol. 705 (American Institute of Physics, Melville, NY, 2004), p. 576.

[29] M. Niibe, M. Mukai, H. Kimura, and Y. Shoji, in *Synchrotron Instrumentation: Eighth International Conference on Synchrotron Radiation Instrumentation*, AIP Conference Proceedings Vol. 705 (American Institute of Physics, Melville, NY, 2004), p. 243.

[30] M. Niibe, T. Kotaka, and T. Mitamura, J. Phys.: Conf. Ser. **425**, 132008 (2013).

[31] M. Niibe and T. Tokushima, in *Proceedings of the 12th International Conference on Synchrotron Radiation Instrumentation - SRI2015*, AIP Conference Proceedings Vol. 1741 (American Institute of Physics, Melville, NY, 2016), p. 030042.

[32] P. Hohenberg and W. Kohn, Phys. Rev. B **136**, 864 (1964).

[33] W. Kohn and L. J. Sham, Phys. Rev. A **140**, 1133 (1965).

[34] G. Kresse and J. Furthmuller, Phys. Rev. B **54**, 11169 (1996).

[35] G. Kresse and D. Joubert, Phys. Rev. B **59**, 1758 (1999).

[36] J. P. Perdew, K. Burke, and M. Ernzerhof, Phys. Rev. Lett. **77**, 3865 (1996).

[37] V. I. Anisimov, J. Zaanen, and O. K. Andersen, Phys. Rev. B **44**, 943 (1991).

[38] H. J. Monkhorst and J. D. Pack, Phys. Rev. B **13**, 5188 (1976).
[39] I. Jimenez, A. Jankowski, L. J. Terminello, J. A. Carlisle, D. G. J. Sutherland, G. L. Doll, J. V. Mantese, W. M. Tong, D. K. Shuh, and F. J. Humpsel, Appl. Phys. Lett. **68**, 2816 (1996).
[40] J. Iihara, Y. Muramatsu, T. Takebe, A. Sawamura, A. Namba, T. Imai, J. D. Denlinger, and C. C. Perera, Jpn. J. Appl. Phys. **44**, 6612 (2005).
[41] M. E. Fleet and X. Liu, Phys. Chem. Miner. **28**, 421 (2001).
[42] M. Niibe, K. Miyamoto, T. Mitamura, and K. Mochiji, J. Vac. Sci. Technol., A **28**, 1157 (2010).
[43] C. B. Stagarescu, L. C. Duda, K. E. Smith, J. H. Guo, J. Nordgren, R. Singh, and T. D. Moustakas, Phys. Rev. B **54**, R17335(R) (1996).
[44] L.-C. Duda, C. B. Stagarescu, J. Downes, K. E. Smith, D. Korakakis, T. D. Moustakas, J. Guo, and J. Nordgren, Phys. Rev. B **58**, 1928 (1998).
[45] F. M. F. de Groot, J. Electron Spectrosc. Relat. Phenom. **67**, 529 (1994).
[46] A. Chaiken, L. J. Terminello, J. Wong, G. L. Doll, and C. A. Taylor II, Appl. Phys. Lett. **63**, 2112 (1993).
[47] J. B. MacNaughton, A. Moewes, R. G. Wilks, X. T. Zhou, T. K. Sham, T. Taniguchi, C. Y. Chan, W. J. Zhang, I. Bello, S. T. Lee, H. Hofsass, and K. Watanabe, Phys. Rev. B **72**, 195113 (2005).
[48] A. A. Tonkikh, E. N. Voloshina, P. Werner, H. Blumtritt, B. Senkosskiy, G. Guntherodt, S. S. P. Parkin, and Yu. S. Dedkov, Sci. Rep. **6**, 23547 (2016).
[49] M. Niibe, N. Takehira, and T. Tokushima, e-J. Surf. Sci. Nanotechnol. **16**, 122 (2018).
[50] R. A. Rosenberg, P. J. Love, and V. Rehn, Phys. Rev. B **33**, 4034 (1986).
[51] V. V. Belavin, A. V. Okotrub, L. G. Bulusheva, A. S. Kotosonov, D. V. Vyalykh, and S. L. Molodtsov, J. Exp. Theor. Phys. **103**, 604 (2006).
[52] M. Niibe, T. Tokushima, N. Takehira, and Y. Araki, J. Electron Spectrosc. Relat. Phenom. **220**, 118 (2017).
[53] D. Usachov, V. K. Adamchuk, D. Haberer, A. Gruneis, H. Sachdev, A. B. Preobrajenski, C. Laubschat, and D. V. Vyalikh, Phys. Rev. B **82**, 075415 (2010).
[54] S. Suzuki, Y. Haruyama, M. Niibe, T. Tokushima, A. Yamaguchi, Y. Utsumi, A. Ito, R. Kadowaki, A. Maruta, and T. Abukawa, Mater. Res. Express **6**, 016304 (2019).
[55] A. B. Preobrajenski, S. A. Krasnikov, A. S. Vinogradov, M. L. Ng, T. Kaambre, A. A. Cafolla, and N. Martensson, Phys. Rev. B **77**, 085421 (2008).
[56] C. Shekhar, A. N. Nayak, Y. Sun, M. Schmidt, M. Nicklas, I. Leermakers, U. Zeitler, Y. Skourski, J. Wosnitza, Z. Liu, Y. Chen, W. Schnelle, H. Borrman, Y. Grin, C. Felser, and B. Yan, Nat. Phys. **11**, 645 (2015).
[57] X. Huang, L. Zhao, Y. Long, P. Wang, D. Chen, Z. Yang, H. Liang, M. Xue, H. Weng, Z. Fang, X. Dai, and G. Chen, Phys. Rev. X **5**, 031023 (2015).
[58] *2D Boron: Boraphene, Borophene, Boronene*, edited by I. Matsuda and K. Wu (Springer, New York, 2021).